Computers and Concrete, *Vol. 16, No. 4 (2015) 503-529*
DOI: http://dx.doi.org/10.12989/cac.2015.16.4.503

Incorporation preference for rubber-steel bearing isolation in retrofitting existing multi storied building

A.B.M. Saiful Islam[1], Mohd Zamin Jumaat[1], Raja Rizwan Hussain[*2], Md. Akter Hosen[1] and Md. Nazmul Huda[1]

[1]Department of Civil Engineering, University of Malaya, Kuala Lumpur, Malaysia
[2]CoE-CRT, Department of Civil Engineering, College of Engineering, King Saud University, Riyadh, Saudi Arabia

(Received April 8, 2014, Revised January 1, 2015, Accepted July 26, 2015)

Abstract. Traditionally, multi-story buildings are designed to provide stiffer structural support to withstand lateral earthquake loading. Introducing flexible elements at the base of a structure and providing sufficient damping is an alternative way to mitigate seismic hazards. These features can be achieved with a device known as an isolator. This paper covers the design of base isolators for multi-story buildings in medium-risk seismicity regions and evaluates the structural responses of such isolators. The well-known tower building for police personnel built in Dhaka, Bangladesh by the Public Works Department (PWD) has been used as a case study to justify the viability of incorporating base isolators. The objective of this research was to establish a simplified model of the building that can be effectively used for dynamic analysis, to evaluate the structural status, and to suggest an alternative option to handle the lateral seismic load. A finite element model was incorporated to understand the structural responses. Rubber-steel bearing (RSB) isolators such as Lead rubber bearing (LRB) and high damping rubber bearing (HDRB) were used in the model to insert an isolator link element in the structural base. The nonlinearities of rubber-steel bearings were considered in detail. Linear static, linear dynamic, and nonlinear dynamic analyses were performed for both fixed-based (FB) and base isolated (BI) buildings considering the earthquake accelerograms, histories, and response spectra of the geological sites. Both the time-domain and frequency-domain approaches were used for dynamic solutions. The results indicated that for existing multi-story buildings, RSB diminishes the muscular amount of structural response compared to conventional non-isolated structures. The device also allows for higher horizontal displacement and greater structural flexibility. The suggested isolation technique is able to mitigate the structural hazard under even strong earthquake vulnerability.

Keywords: structural retrofitting; seismic isolation; existing building; rubber-steel bearing; frequency domain; time domain analysis; LRB; HDRB; innovative model

1. Introduction

In recent decades, seismic isolation has been increasingly implemented around the world, and it has proven helpful for earthquake safety. The separation of the structure from the harmful motions

*Corresponding author, Professor, E-mail: raja386@hotmail.com

http://www.techno-press.org/?journal=cac&subpage=8 ISSN: 1598-8198 (Print), 1598-818X (Online)

of the ground is accomplished by providing flexibility and energy dissipation through the insertion of isolators between the foundation and building structure (Ismail *et al.* 2010). New, clever approaches, such as base isolation (BI), are becoming more popular than the widely adopted seismic strengthening technique (Lee *et al.* 2013). Most of the seismic energy that would be transferred to the structure is absorbed at the base level through isolation. Moreover, the frequency of movement in the BI structure is reduced compared to the shaking of a typical earthquake. Traditional designs are based on increasing resistance by strengthening the structure; seismic isolation seeks to reduce the dynamic loading exhibited by earthquake motion in a structural base (Ahmad *et al.* 2009, Ates and Yurdakul 2011).

Rubber-steel bearing (RSB) isolators, such as lead rubber bearings (LRBs, 1970s) and high-damping rubber bearings (HDRBs, early 1980s) represent a new implementation of BI in structures (Ates 2012, Islam *et al.* 2012a, Lu and Lin 2008). Dall'Asta and Ragni (2006, 2008) have performed experiments, developed models, and analyzed the nonlinear dynamic behavior of HDRBs. Providakis (2008) explored the responses of aseismic multi-story buildings isolated by LRBs at near-fault motion. This innovative seismic isolation system for multi-story buildings has been evaluated and its advancement is reviewed by several investigators (Baratta and Corbi; Hong and Kim 2004, Islam *et al.* 2013b, Islam *et al.* 2012b). Base isolators with hardening behavior under increasing loading have been reported for medium-rise buildings with moderate earthquake risk (Pocanschi and Phocas 2007). Ariga *et al*. (2006) evaluated the resonant behavior of BI high-rise buildings under long-period ground motions. Islam *et al*. (2014) studied the effectiveness of base isolation to mitigate the soft story phenomena in tall building, In addition, Olsen *et al*. (2008) studied the long-period responses of buildings with isolators. Dicleli and Buddaram (2007), Casciati and Hamdaoui (2008), and Islam *et al*. (Islam *et al.* 2013a) evaluated isolation system for multi-story buildings by using a number of HDRB and LRB categories. Roy and Chakraborty (2013) presented optimal design of base isolation system considering uncertain bounded system parameters. A number of studies on mitigating the seismic effects of historic structures have also demonstrated the usefulness of incorporating isolation systems (Anzani *et al.* 2010, Ates 2012, Borzi *et al*. 2013, Gürsoy 2014, Xue and Yang 2014).

Prominent structures in Dhaka, Bangladesh, are good candidates for being made flexible by the insertion of an isolator. The earthquake disaster risk index has placed the medium-risk seismic region Dhaka among the 20 most vulnerable cities in the world. The recently measured plate motions at six different sites in Bangladesh, including Dhaka, clearly demonstrate that Dhaka is moving 30.6 mm/year in the northeast direction. Furthermore, the relatively high rate of strain accumulation in and around Dhaka may precipitate an earthquake of magnitude 6.8 (Khan and Hossain 2005). Buildings experience time-varying loads when subjected to such strong earthquake excitations. The seismic considerations of building designs in Dhaka are typically based on the traditional approach. Major earthquakes reported in the literature have shown that ductile structures provide unsatisfactory performance (Iriarte *et al.* 2010). Seismic isolation is one of the most promising alternatives to improve the performance of these structures. This type of structural system can be implemented for new structures and can also be retrofitted to existing buildings. The dynamic characteristics of the base isolator are designed to uncouple the base from ground motion.

Few reports have studied the option of incorporating RSB devices in medium-risk seismic regions. The relatively complex time-domain method and rapid frequency-domain method have not been adopted simultaneously under bidirectional site-specific earthquake loading. In this study, we model the configuration of HDRBs and LRBs and explore the suitability of incorporating isolators using equivalent static analysis. The study area (Dhaka, Bangladesh) is used as a

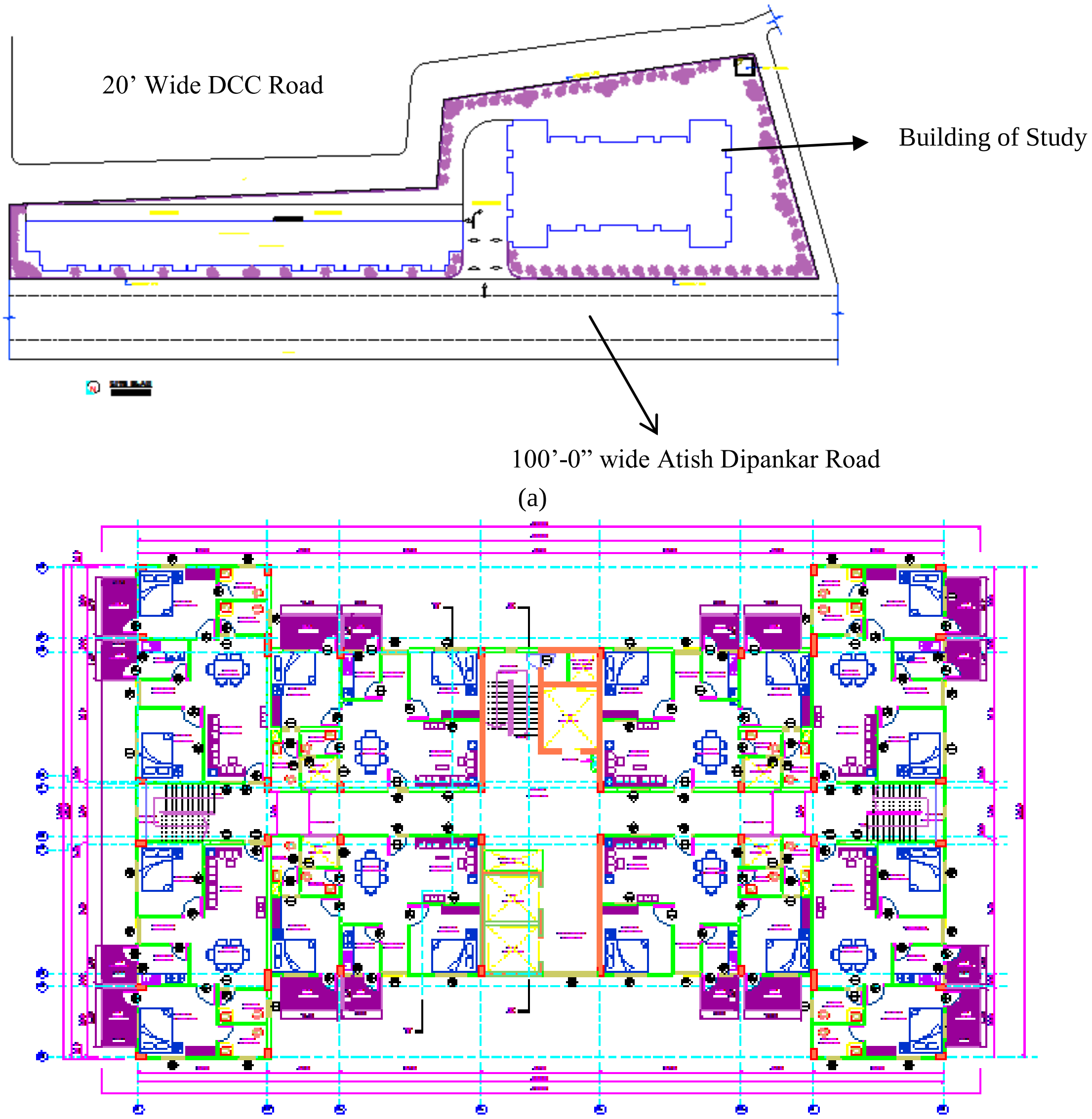

(a)

(b)

Fig. 1 Site location map (a) and architectural plan (b) of the building

representative medium-risk seismic region. We present the development of a finite element model. We also present static analysis and free vibration analysis (Betti and Vignoli 2011, Ozmen *et al.* 2013), along with dynamic analysis in the frequency and time domains. The acceleration excitation behaviors for fixed-base (FB) and BI buildings are assessed with the displacement patterns at different levels. In addition, base shear and overturning moments are compared for both the FB and BI cases. Every comparison is supported by comparison to the maximum and minimum structural excitation values. Significant reductions in the structural responses are observed. Furthermore, the flexibility of the modeled structures is shown to be increased through seismic BI.

2. Structural model

A moment-resisting reinforced-concrete frame structure was retained for the existing multi-story building model. The superstructure was simulated using a linear elastic system for the conventional FB building. The multi-story building structure is shown in Fig. 1. RSBs are incorporated between the foundation and superstructure, and nonlinear behavior is confined to the RSB isolators. The base and floors of the multi-story building are assumed to be infinitely rigid. The structural system follows these additional assumptions:

1) The superstructure and base of the building have been configured using six degrees of freedom at the center of mass of each floor.

2) The superstructure behaves elastically and inelastically during earthquake excitation.

3) Floors are considered rigid in their own plane, and the masses for each floor are added together.

4) The entire structure is excited by the bidirectional components of earthquake ground motion (x- and y-directions).

5) Base isolators convey the vertical load but undergo no vertical deformation.

6) A bilinear model is used to simulate the LRBs, and the equivalent linear model is used for the HDRBs.

7) The RSBs are fixed at the bottom to the foundation and at the top to the base mass.

2.1 Numerical formulation

BI structures require dynamic analysis because of their complexity. Here, the ETABS (Habibullah 2007) program was used for static and dynamic analyses assuming a linear elastic structure. The HDRB and LRB isolators were designed with different properties as part of the static design procedure. The bearings were linked at the base of the buildings and analyzed accordingly. Dynamic analysis in the frequency domain was performed for both the FB and BI cases. Bearings were designed with the program DESBEA11, which was used to formulate the equations and conditions.

2.2 Modeling of isolators

A hysteresis model was designed to provide stiffness and resistance under any displacement history. In addition, the basic characteristics were defined through member geometry and material properties. To carry out response spectrum analysis, the effective stiffness (K_{eff}) and equivalent viscous damping, derived from the isolator's energy dissipated per cycle (EDC), are essential. The force-deformation behaviors of the isolators in this study were modeled as follows for the LRBs and HDRBs:

(a) LRB: Nonlinear hysteretic loop directly specified by the bilinear model.

(b) HDRB: Equivalent linear elastic model with viscous damping included for the nonlinear system.

2.2.1 Bilinear LRB model

An LRB is formed by force-fitting a lead plug into a preformed hole in a low-damping elastomeric bearing, as shown in Fig. 2(a). The basic components of such bearings are rubber and steel plates, constructed in alternating layers. The steel plates force the lead plug in the bearing to

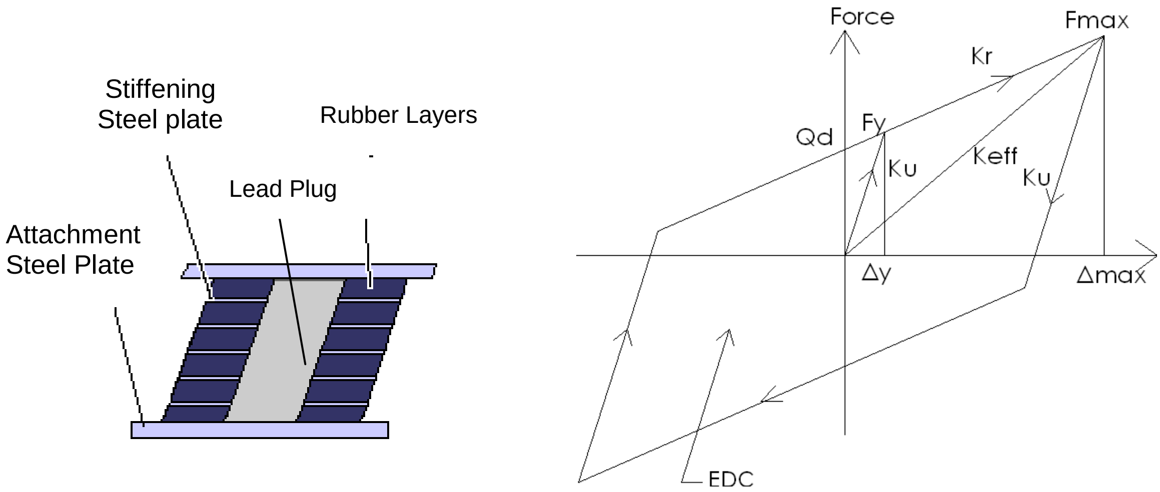

(a) (b)

Fig. 2 LRB: (a) Deformation pattern; (b) Idealized Bi-linear hysteretic model

deform and shear. The LRB system offers the parallel action of linear springing and damping. The system decouples the structure from the horizontal components of earthquake ground motion by interjecting a layer of low horizontal stiffness between the foundation and superstructure. Generally, the LRB exhibits the required amount of damping, horizontal flexibility, and vertical stiffness. Large differences in the damping of the structure and isolation device make the system non-classically damped, leading to the coupling of the equations of motion. An elastic, perfectly plastic hysteretic model was used to consider the essential isolation characteristics, and this model is referred to as the bilinear model. The model is constructed using the standard bilinear hysteretic rules with kinematic strain hardening. Its behavior varies according to the yield point load for the lead core, horizontal stiffness (lead core contribution), and horizontal stiffness (elastomer contribution). The nonlinear force deformation behavior of the RSB is modeled by the bilinear hysteretic model, which is controlled by the characteristic strength, post-elastic stiffness, and yield displacement. An idealized hysteresis for the bearing is shown in Fig. 2(b). The force intercept at zero displacement in hysteresis, Q_d, also termed the characteristic strength, is correlated with yield strength.

$$Q_d = \sigma_y A_{pl} \tag{1}$$

In this equation, the yield strength, σ_y, is dependent on the vertical load and lead core confinement.

The post-elastic stiffness is defined as

$$K_r = \frac{G_\gamma A_r}{T_r} \tag{2}$$

The elastic (or unloading) stiffness (Kilar and Koren 2009) is defined as

$$K_u = 6.5 K_r \left(1 + \frac{12 A_{pl}}{A_r}\right) \tag{3}$$

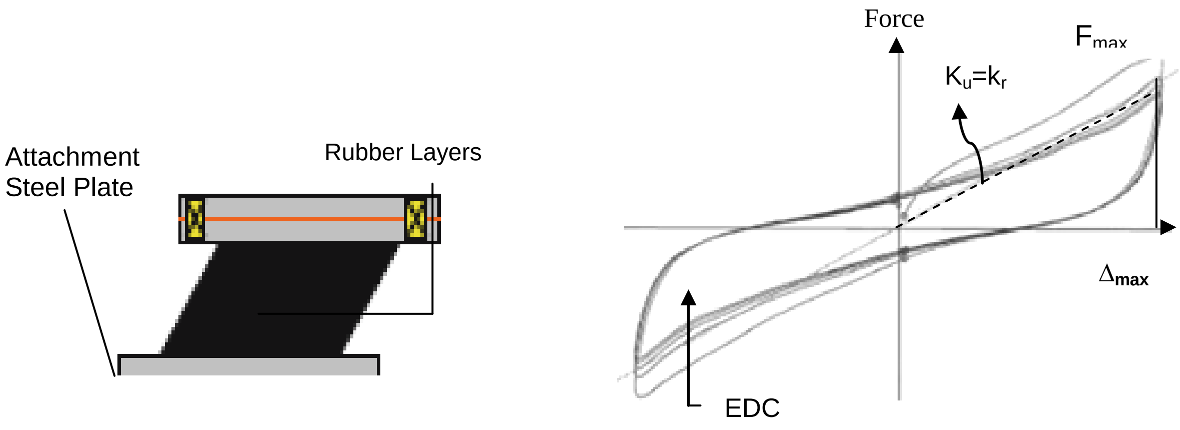

(a) (b)

Fig. 3 HDRB: (a) Deformation pattern; (b) Equivalent linear hysteretic model

W is the weight of the structure, which can be used to define a bilinear model. The ratio of post-yield stiffness and elastic stiffness varies within a small range, 0.08-0.12, for the LRBs. When the peak displacement of a bilinear model is larger than the yield displacement, the lateral shear force, *F*, and effective stiffness, K_{eff} (secant stiffness), at peak displacement for a bilinear system can be calculated as follows:

Effective stiffness

$$K_{eff} = \frac{F_m}{\Delta} \tag{4}$$

$$F_m = Q_d + K_r \Delta \tag{5}$$

Effective period

$$T_e = 2\pi \sqrt{\frac{W}{g \sum K_{eff}}} \tag{6}$$

Equivalent viscous damping

$$\beta = \frac{1}{2\pi} \left(\frac{A_h}{K_{eff} \Delta^2} \right) \tag{7}$$

LRB isolators are strongly nonlinear, i.e., the parameters K_{eff} and β are valid only for the design displacement, $\Delta_{max.}$ The maximum isolator displacement is thus given by

$$\Delta_m = \frac{S_a T_e^{\,2}}{4\pi^2 B} \tag{8}$$

where S_a is the spectral acceleration at T_e

F_m=F_{max} is the maximum force, F_y is the yield force, Δ_y is the yield displacement, *EDC* is the energy dissipated per cycle, and A_h is the area of the hysteresis loop

2.2.2 Equivalent linear HDRB model

An HDRB consists of thin layers of high-damping rubber and steel plates fabricated in alternating layers, as illustrated in Fig. 3(a). The low shear modulus of the elastomer controls the horizontal stiffness of the bearing. The steel plates provide high vertical stiffness and prevent bulging of the rubber. Horizontal stiffness is not affected by the high vertical stiffness for such a RSB. Damping in the isolation system is increased by adding extra-fine carbon blocks, oils, resins, and other proprietary fillers. The parallel action of the linear spring and viscous damping is the dominant feature of the HDRB system. Furthermore, the damping in this bearing model is neither viscous nor hysteretic. HDRB uses a lower stiffness to obtain a higher natural period. An equivalent linear elastic viscous damping model was chosen to configure the HDRB (Fig. 3(b)). The non-linear force-deformation characteristic of the RSB is swapped through effective elastic stiffness and effective viscous damping. In this model:

• Instead of K_r, stiffness is expressed as the effective horizontal stiffness K_{eff}.

• Damping is considered as effective viscous damping.

The equations required to model the HDRB follows Eqs. (2) and (4)-(8). The elastic (or unloading) stiffness is defined as follows

$$K_u = K_r \tag{9}$$

2.3 Lateral static loading

Linear static analysis, the simplest of all the analyses, represents a minimum level of complexity. Seismic lateral load was determined by choosing *Z*, *R*, and the soil profile, among other factors. Furthermore, the lateral load for wind was obtained from the related coefficients. The formula for earthquake and wind analysis was taken from Bangladesh National Building Code (BNBC) (1993)as follows

$$V_{EQ} = ZIC / R \tag{10}$$

The base shear for earthquake loading is $V_{EQ.}$ The seismic zone factor is denoted as *Z*. *I* is the importance factor, *R* is the response modification factor, C=1.25$S/T^{2/3}$, *S* is the soil structure interaction, *T* is the structural time period, and W is the effective weight of the structure.

$$(P_z)_W = C_G C_P C_C C_I C_Z v_b{}^2 \tag{11}$$

The design wind pressure at varying height is $(P_z)_{W.}$ C_C is the conversion coefficient from velocity to pressure, C_I is the structure importance coefficient, C_Z is the combined height and exposure coefficient, v_b is the basic wind speed, C_G is the gust coefficient, and C_p is the pressure coefficient.

2.4 Equations of motion

The equations of motion of the super structure for all BI systems can be derived as follows

$$[M]\{\dot{y} + \ddot{y}_b\} + [C]\{\dot{y}\} + [K]\{y\} = -[M][T_g]\{\ddot{u}_g\} \tag{12}$$

[M], [K] and [C] are the mass, damping and stiffness matrices of the superstructure, respectively. $\{y\}=[y_x, y_y, y_z]^T$ is the displacement vector at the slab, which is related to the base mass. $\{y_b\}=[y_{bx},y_{by},y_{bz}]^T$ is the vector of base displacements relative to the ground. $\{\ddot{u}_g\}$ is the ground acceleration vector, and $[T_g]$ is the earthquake influence coefficient matrix.

2.5 Dynamic solution

2.5.1 Time-domain analysis

Nonlinear time-domain analysis was performed in the sophisticated package. The P-delta effect was considered for geometric nonlinearity. Material nonlinearity, along with link nonlinearity, was also included. Direction integration was performed by the Hilber-Hughes-Taylor Alpha method. The nonlinearities were restricted to the nonlinear link elements. The above dynamic equilibrium equations, which consider the super structure to be elastic and the link to be nonlinear, can be written as

$$[M]\{\ddot{y}(t)+\ddot{y}_b(t)\}+[C]\{\dot{y}(t)\}+[K_L]\{y(t)\}+r_N(t)=r(t)-[r_N(t)-K_N y(t)]) \tag{13}$$

The stiffness matrix K is the sum of K_L and kN. K_L is the stiffness matrix for all of the linear elements, K_N is the stiffness matrix for all of the nonlinear degrees of freedom, r_N is the vector of forces from the nonlinear degrees of freedom in the gap elements, y, $\dot{y}$, and $\ddot{y}$ are the relative displacement, velocity, and acceleration with respect to the ground, respectively, and r is the vector of applied loads. The effective stiffness at the nonlinear degrees of freedom is arbitrary but varies between zero and the maximum stiffness of that degree of freedom.

The fast nonlinear analysis (FNA) technique was used to solve the equilibrium equations. This technique is extremely efficient, as it is designed for structural systems that are primarily linear-elastic but have a limited number of predefined nonlinear elements. For the FNA method, all nonlinearities are restricted to the link elements. The specific time-history load is applied quasi-statically with high damping. The FNA considers a ramp type of time-history function that increases linearly from zero to one over a length of time. The nonlinear equations are solved iteratively in each time step. The program allows the analysis results to vary during a time step. The iterations are carried out until the solution converges. If convergence cannot be achieved, the program divides the time step into smaller sub-steps and tries again.

2.5.2 Frequency-domain analysis

Dynamic frequency-domain analysis is required for systems with unproportional damping, hysteric properties, and frequency-dependent properties. The approach offers computational advantages in the prediction of the displacements, velocity, and acceleration of the ground subjected to structural systems (Islam *et al.* 2013a). Equations of motion for linear analysis are transformed into a normal coordinate system. Applying the normal coordinate transformation to the decoupled equation of motion for individual modes leads to the following

$$[M_n]\{\ddot{y}(t)_n+\ddot{y}_b(t)_n\}+[C_n]\{\dot{y}(t)_n\}+[K_n]\{y(t)_n\}=-[M][T_g]\{\ddot{u}(t)_g\} \tag{14}$$

The solution can be obtained individually for each decoupled modal equation by using Eq. (15), where ζ is the modal damping ratio and ω_n is the undamped natural frequency.

$$\ddot{y}(t)_n+2\zeta\omega_n\dot{y}(t)_n+\omega_n{}^2 y(t)_n=-\ddot{u}(t)_g \tag{15}$$

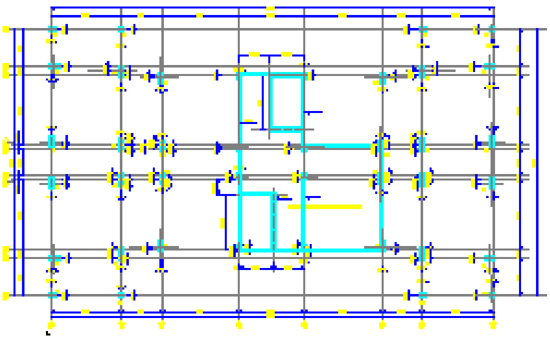

Fig. 4 Column layout plan of the building

The total acceleration of the unit mass in a single-degree-of-freedom system, governed by Eq. (15), is given by

$$\ddot{u}(t)_T = \ddot{y}(t) + \ddot{u}(t)_g \tag{16}$$

Eq. (15) can be solved for $y(t)$. Substituting the term into Eq. (16) yields

$$\ddot{u}(t)_T = -2\zeta\omega\,\dot{y}(t) - \omega^2 y(t) \tag{17}$$

The maximum modal displacement can be obtained for a typical mode n with period T_n and the corresponding spectrum response value $S(\omega_n)$. The maximum modal response associated with period T_n is calculated by Eq. (18), and the maximum modal displacement response is calculated by Eq. (19).

$$y(T_n)_{MAX} = S(\omega_n)/\omega^2 \tag{18}$$

$$u_n = y(T_n)_{MAX}\,\Phi_n \tag{19}$$

The frequency-domain analysis was performed using the aforementioned method of mode superposition. The modal values were combined using the complete quadratic combination (CQC) technique. Directional combination was performed by the SRSS method.

3. Numerical analysis

The 10-story residential tower building for police personnel consists of four 800-ft^2 apartments on each floor. The project area is 3,524.67 m^2, and there are two 10-story buildings, Tower 1 and Tower 2, at the perimeter. Tower 1 and Tower 2 occupy areas of 663.315 m^2 and 757.380 m^2, respectively. Tower 2 was considered for the case study in this research. Police Tower-2 is supported on 32 columns and six shear walls. Four types of columns were considered, C1, C2, C3, and C4; there are eight, 12, four, and eight C1-C4-type columns in the building under consideration, respectively. Three types of shear walls were considered, SW1, SW2, and SW3; There are two, one, and one SW1-SW3-type shear walls, respectively. The column layout in the building is shown in Fig. 4. Some different views of the building are shown in the Appendix (Figs. A1-A4).

Table 1 Salient feature of the building

Parameter	Rating
Length (X-direction)	40.80 m
Width (Y-direction)	23.00 m
Number of Span in X-direction	07
Number of Span in Y-direction	05
Length of span in X-direction	6.75 m (maximum)
Length of span in Y-direction	6.15 m (maximum)
Covered Area of the Building	757.380 m^2
No. of Shear Walls	4
Total No. of Columns	32
Total No. of Piles	340
Average Length of Pile	10.5 m
No. of Lift	02
No. of Void	04

The features are summarized in Table 1, which lists different attributes of the Tower 2. The floor slabs were cast *in situ* using reinforced concrete with a varying depth. The average depth is 140 mm. All slabs are two way and monolithic, with a beam column frame.

From a seismic response perspective, the four elements of the building (floors, columns, shear walls, and piles) are important. Thus, we provide further descriptions of the configurations and properties of these elements.

3.1 Pile configuration

The substructure consists of four piles with a 1.87×1.87-m pile cap under eight single columns, eight piles with a 1.87×3.97-m pile cap under four single columns, nine piles with a 2.92×2.92-m pile cap under four single columns, 10 piles with a 2.92×3.97-m pile cap under four single columns, 16 piles with a 2.92×6.07-m pile cap under two double columns, 18 piles with 2.92×6.17-m pile cap under two double columns, and 20 piles with 3.98×5.02-m pile cap under two double columns. Each pile is 350×350 mm and 12.00 m long. There are 92 350×350-mm, 9.00-m-long piles under the shear walls. All of the piles are precast and filled with concrete. The top level of piles varies from -2.53 m for the 9.00-m piles to -0.50 m for the 12.00-m piles. The pile caps have a cast *in situ* reinforced concrete infill construction. The pile caps under the columns have a top level of -0.5 mm, so the piles are embedded 305 mm within the caps. Fig. 5a presents the cross section of a maximally loaded column with a pile cap.

3.2 Column configuration

Four types of columns were considered: C1 (450×1,000 mm), C2 (450×950 mm), C3 (450×900 mm), and C4 (425×500 mm). The columns rest on pile caps (ground floor size). The columns are 3.0 m and constructed with reinforced concrete. Fig. 5(a) presents a vertical section of a maximally loaded column. The cross-sectional properties of the columns are provided in Table 2.

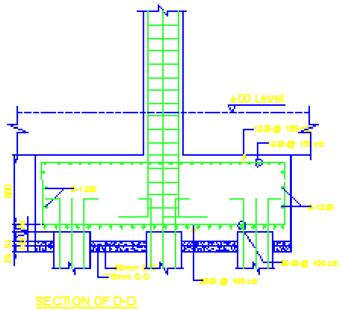

(a)

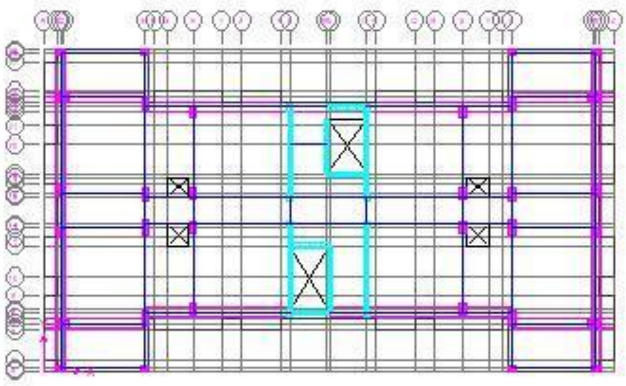

(b)

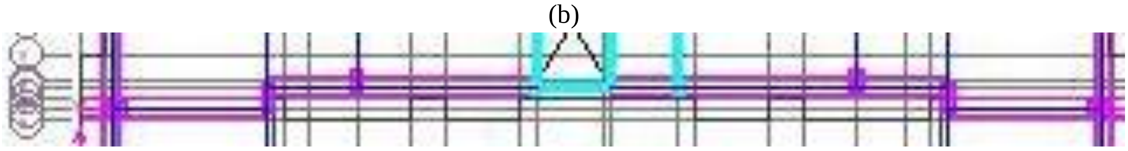

(c)

Fig. 5 Typical plan of the building and section of maximum loaded column (a) Section of column C1 over 10-piled pile cap, (b) Typical layout plan of the building, (c) Partial plan showing grid line through Column C1

Table 2 Cross-sectional properties of columns

Section Type	Area m^2	Moment of Inertia I_x (m^4)	Moment of Inertia I_y (m^4)
C1 (450 mm×1000 mm)	0.45	0.0375	0.007594
C2 (450 mm×950 mm)	0.4275	0.032152	0.007214
C3 (450 mm×900 mm)	0.405	0.027338	0.006834
C4 (425 mm×500 mm)	0.2125	.004427	0.003199

3.3 Shear wall configuration

Three types of elongated columns, i.e., shear walls, are constructed here as SW1 (one wall, 400×6,883 mm), SW2 (four walls of varying dimensions), and SW3 (four walls of varying dimensions), all of which rest on pile caps (ground floor size). The shear walls are 3.0 m tall (from floor to floor) and are constructed by reinforced concrete. Figs. 5(b) and 5(c) illustrate the shear walls adjacent to the void spaces.

3.4 Modeling of the example building

The building consists of seven spans in the *x*-direction and five spans in the *y*-direction. Fig. 5(b) presents the typical layout of the building, with a partial grid plan through column C1. The floor slabs are attached monolithically to the beam columns. The model for the building structure was established as a moment-resisting frame with a response modification factor R=8.5 for the non-isolated structure. The time period of the structure, which denotes the value for the first mode shape, is T=0.5241 s.

3.4.1 Base shear for earthquake and wind loads

Because the building is 45.73 m high, the wind load plays an important role, along with the seismic load. Nevertheless, lateral seismic load is dominant for both shear and moment in both directions, as shown in Table 3.

3.4.2 Sustained load

The seismic weight of the building was considered to be the total load at the base from dead and live loads. The value is W=148,183.8 kN. A maximally loaded column experiences 4,399.34 kN of vertical force, which is the optimum value. This load is an extreme imposed load from the dead and live loads.

3.4.3 Design earthquake

The design earthquake for the dynamic analysis of Tower 2 comes from a generated time history for Dhaka. In this time history, the total time is 30 s, with a time interval of 0.005 s. Thus, there are a total of 6,000 steps. Fig. 6 presents the time-history curve (Islam *et al.* 2013c).

The response spectrum for the 5% damping ratio for this earthquake was considered as part of the response spectrum analysis. Fig. 7 presents the response spectrum curve (Islam *et al.* 2011) in terms of *g*.

3.5 Insertion of an isolation device

To withstand the lateral seismic load, an isolation device was incorporated into the model. Two types of isolator bearings, LRBs and HDRBs, were considered for use at the base of the superstructure. Such devices isolate the superstructure from the substructure, thus changing the displacement behavior and reducing the values of different forces.

There are 46 isolation devices for this building. Fig. 8 presents the load-displacement curves determined from the spreadsheet for the LRBs and HDRBs. The properties are reported in Table 4.

Table 3 Base shear and moment for lateral load

	W_X (KN)	W_Y (KN)	EQ_X (KN-m)	EQ_Y (KN-m)
Base Shear	3215.40	6114.345	5122.44	6290.62
Base Moment	81344.173	155188.498	167514.61	203950.859

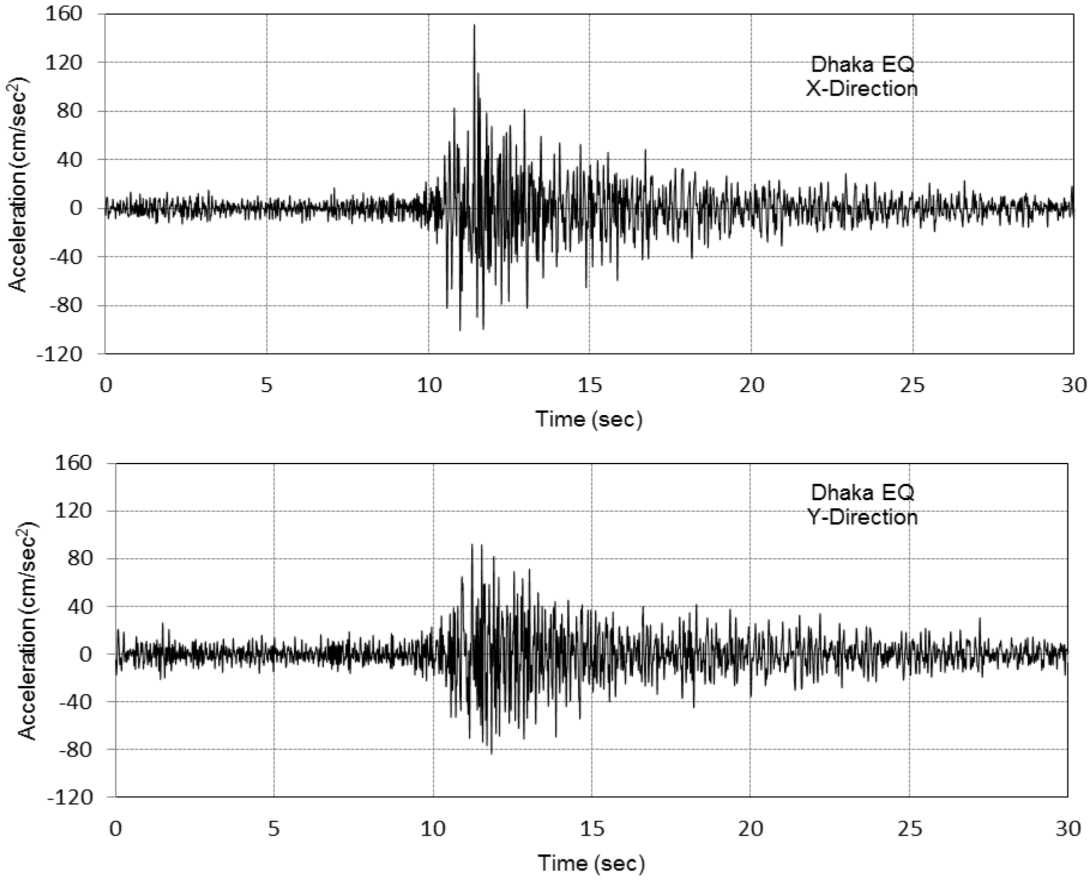

Fig. 6 Selected time history for Dhaka *EQ* in *X*-direction (top) and *Y*-direction (bottom)

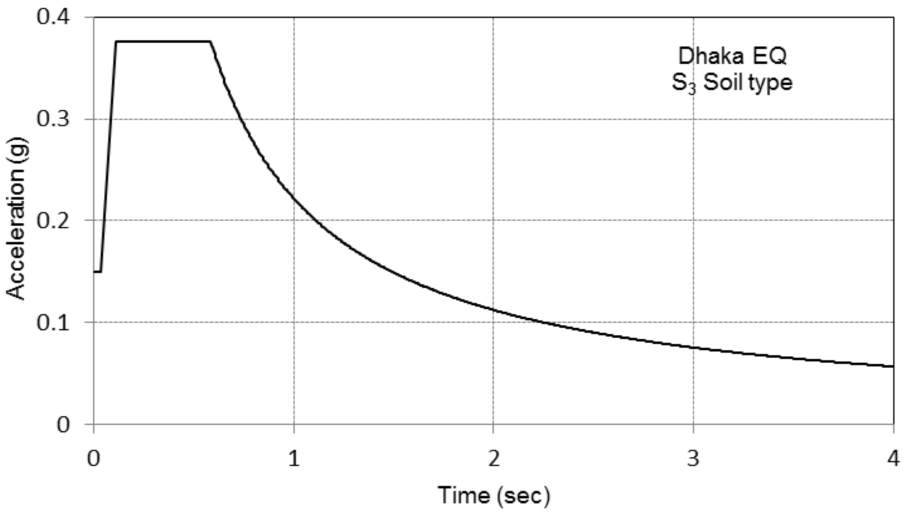

Fig. 7 Selected acceleration response spectrum for Dhaka EQ

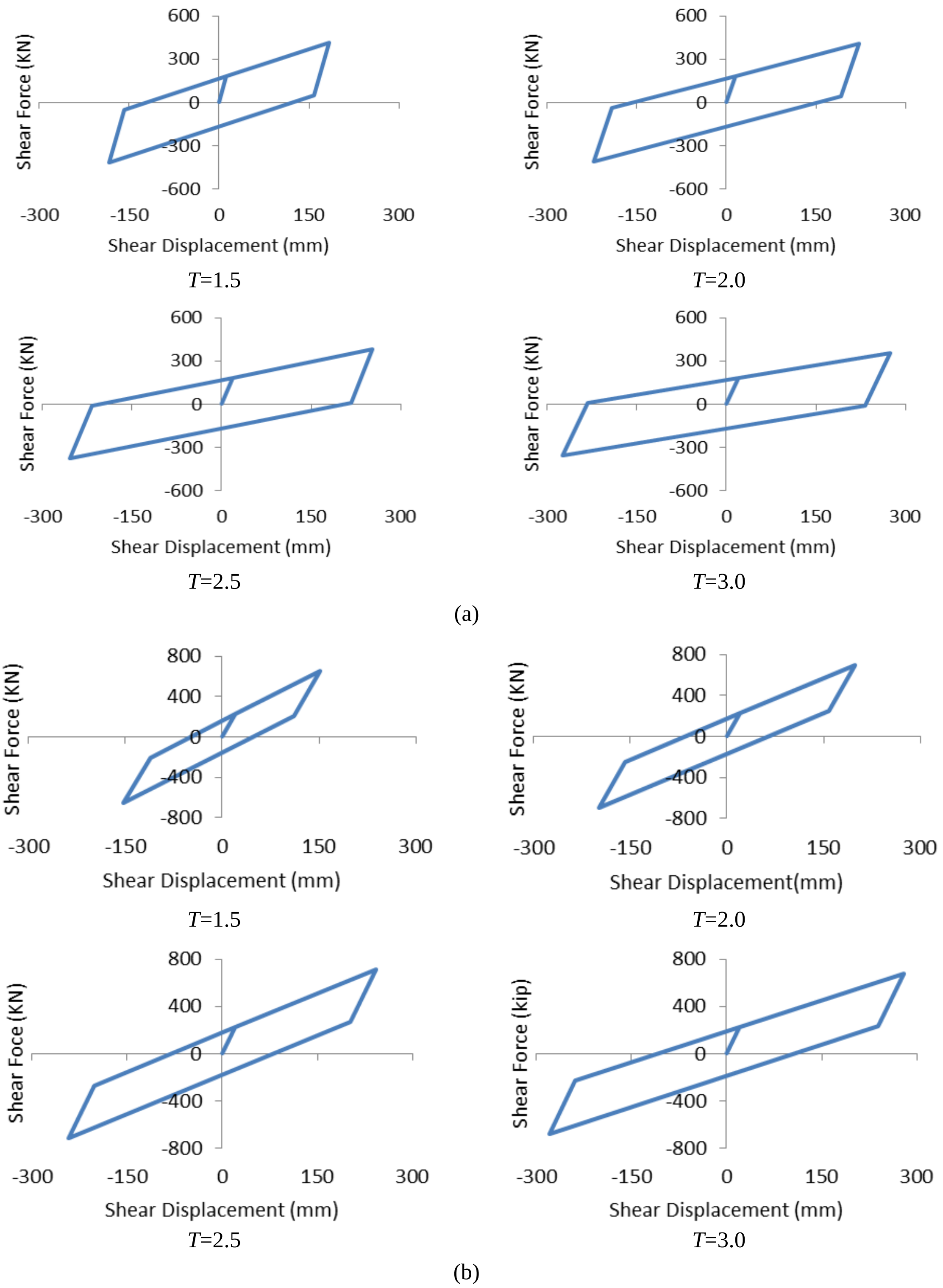

Fig. 8 Hysteresis curve of the isolation device: (a) lead rubber bearings, (b) high damping rubber bearings

Table 4 Force-displacement relationship of optimum isolation device

Isolator Type	Force Elastic (KN)	Elastic Displacement (mm)	Force Plastic (KN)	Plastic Displacement (mm)
LRB	338.87	23.62	553.31	183.13
HDRB	222.14	20.32	713.85	242.57

Table 5 Isolation system variations

System Variation	Isolated Period (sec)	β (%)
LRB	1.5	8%
LRB	2	11%
LRB	2.5	15%
LRB	3	20%
HDR	1.5	15%
HDR	2	16%
HDR	2.5	17%
HDR	3	19%

As shown in Fig. 8, the key properties of the isolator are the following:

• Initial Slope of the Isolator, $k_i=k_1$=Initial Stiffness=Elastic Stiffness=14.45 kN/mm for the LRBs and 10.91 kN/mm for the HDRBs.

• Post-Yielding Slope of the Isolator, $k_h=k_2$=Post-Yielding Stiffness=1.40 kN/mm for the LRBs and 1.78 kN/mm for the HDRBs.

The diameter of the isolators was set to a default value of 850 mm, and there were 16 layers for both the LRBs and HDRBs.

For the LRBs, the force intercept Qd was taken to be 5% of the seismic load. For the HDRBs, this characteristic strength is dependent on the damping properties. Damping has been considered as stated in Table 5.

4. Results and discussion

The present study incorporates different kind of rubber steel bearing (RSB) isolation like LRB and HDRB as the alternative device of solution for mitigating the seismic hazards. There are significant structural responses with the varying stiffness of base isolators. Geometry like diameter of base isolator, numbers of layers also have the influential effect on structural behavior of proposed building. Subsequent section discusses thorough interpretations of dynamic consequences.

4.1 Influence of the isolator properties

The displacement (Δ), base shear (V), and base moment (M) vary with changing properties of RSB. Here, LRBs and HDRBs were considered to establish their influence. For a pre-selected isolator period, several values of the damping ratio (β %) were selected to obtain the initial stiffness (K1), post-yield stiffness (K2), and yield force (F_y), allowing for the comparisons shown

Table 6 System properties for LRB

System Variation Qd=0.050	Isolated Period (sec)	β (%)	Δ (mm)	C	Post-Yield Stiffness Ratio	K1 (KN/mm)	K2 (KN/mm)	F_y KN
LRB	1.5	8%	183.134	0.095	0.0971	14.450275	1.401925	40.10
	2	11%	222.504	0.065	0.0912	12.84465	1.200308	39.85
	2.5	15%	253.238	0.047	0.0844	11.560325	1.038923	39.55
	3	20%	273.558	0.045	0.0796	10.509275	0.906815	39.34

Table 7 System properties for HDRB

System Variation	Isolated Period (sec)	β (%)	Δ (mm)	C	Post-Yield Stiffness Ratio	K1 (KN/mm)	K2 (KN/mm)	F_y KN
HDR	1.5	15%	152.146	0.1049	0.3004	10.912773	1.77625	50.636
	2	16%	198.374	0.1038	0.2479	9.02475	1.54	50.141
	2.5	17%	242.57	0.1034	0.2056	7.6461	1.350825	49.939
	3	19%	279.146	0.1033	0.1628	6.6045	1.196125	49.887

Table 8 Effective stiffness of rubber-steel bearings

System Variation	Isolated Period (sec)	Effective Stiffness (KN/mm)
LRB	1.5	16.63
	2	13.46
	2.5	11.13
	3	9.88
HDR	1.5	31.21
	2	25.83
	2.5	21.86
	3	18.41

in Tables 6 and 7.

4.1.1 Initial stiffness

The elastic stiffness of the LRBs decreases with an increasing damping ratio, with a moderate slope. However, the slope for the HDRBs is very steep, i.e., the initial stiffness decreases significantly with only a minor change in the damping ratio.

4.1.2 Post-yield stiffness

The post-yield stiffness of the LRBs increases with the value of initial stiffness in a concave manner with a nearly linear slope, whereas the increasing curve for the HDRBs is convex. The post-yield stiffness of the HDRBs increases significantly as the initial stiffness increases.

4.1.3 Yield force

For the LRBs, the yield force normalized with the weight of the structure increases rapidly as the value of initial stiffness increases. The increasing slope for the HDRBs is nearly linear, i.e., the increase in the yield force with increases in the initial stiffness remains almost constant.

4.1.4 Effective stiffness

The effective stiffness of the LRBs decreases moderately with the length of the time period for a given characteristic strength. The decreasing slope for the HDRBs is steeper, i.e., the initial stiffness decreases more rapidly with an increasing time period. The effective stiffnesses of the RSBs for different isolator periods are shown in Table 8.

4.2 Influence of the isolator siameter

As the diameter of the LDB increases, the elastic stiffness increases in slightly more rapidly than for HDRB diameter, but the post-yield stiffness increases more slowly. Fig. 9 illustrates how the stiffness varies with the diameter of a LRB with *Qd*=0.05 and *Ti*=1.5.

For increase in diameter of the HDRB, the elastic stiffness increases moderately, but the post-yielded stiffness increases in slower nature. Fig. 10 illustrates how the stiffness varies with the diameter of a HDRB with *Ti*=1.5.

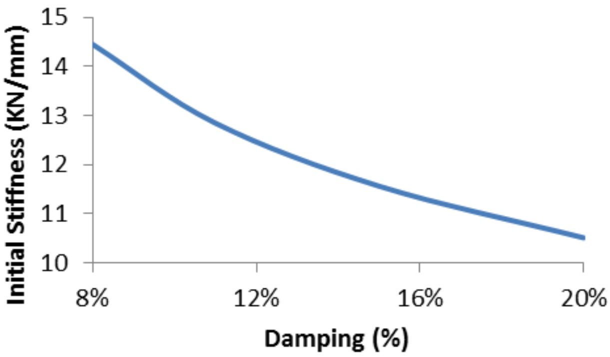

Fig. 9 Initial stiffness vs. damping ratio for LRB

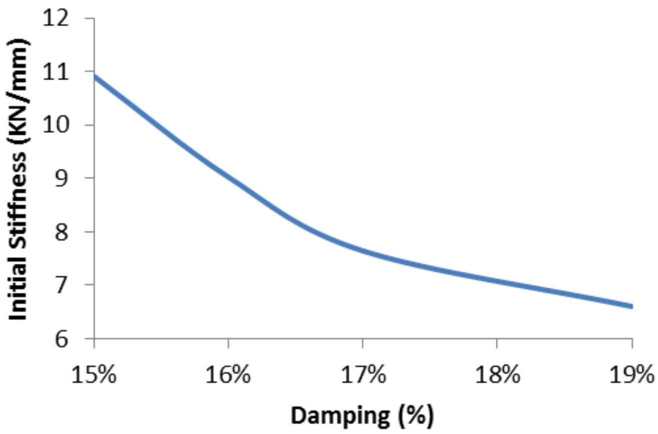

Fig. 10 Initial stiffness vs. damping ratio for HDRB

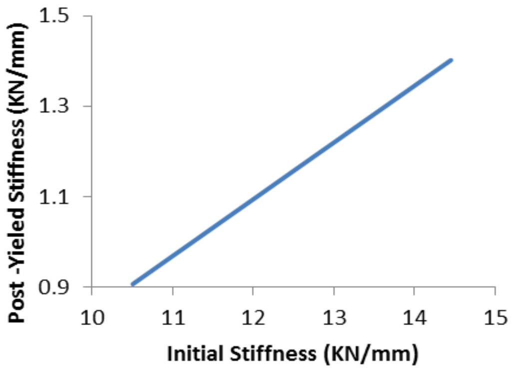

(a) for LRB

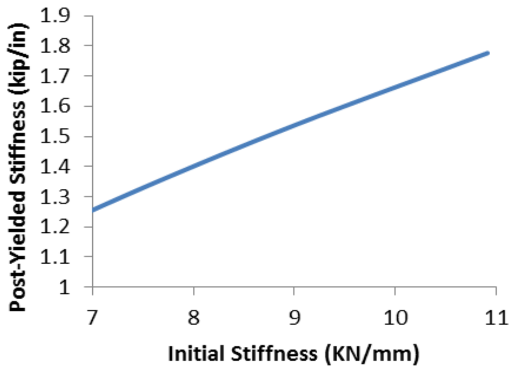

(b) for HDRB

Fig. 11 Post-yielded stiffness vs. initial stiffness

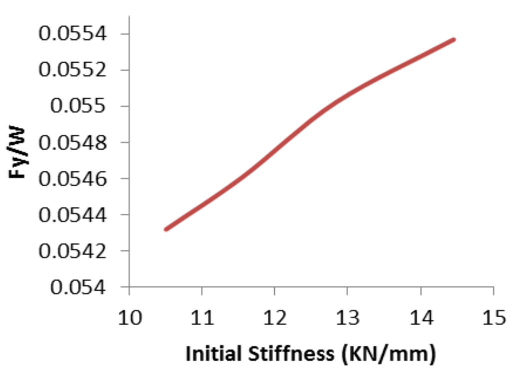

(a) for LRB

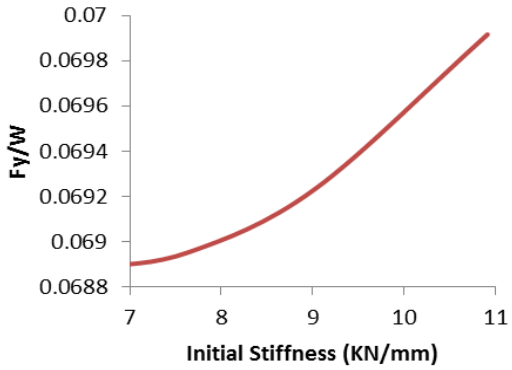

(b) for HDRB

Fig. 12 Normalized yield force with initial stiffness

The post-yield stiffness of the bearings increases linearly with the initial stiffness of the RSBs. Fig. 11 illustrates the variation in stiffness for the LRBs (a) and HDRBs (b). The normalized yield force increases more rapidly as the diameter of the bearing increases for the LRBs than for the HDRBs. Fig. 12 illustrates how the normalized yield force varies with the diameter of the isolator for a) an LRB with *Qd*=0.05 and *Ti*=1.5 and b) an HDRB with *Ti*=1.5. The yield forces have been normalized with the total weight of building. The variation of yield force with varying bearing diameter is observed as quite nonlinear which is conveyed in the illustration.

Detailed comparisons of the stiffness, isolation period, and yield forces for the LRBs and HDRBs are presented in Figs. 13-16. The base shear coefficient (*C*) remains constant for all diameters for the LRB, whereas it increases with an increasing diameter for the HDRBs. Fig. 17 presents the shear coefficient for a LRB with *Qd*=0.05 and *Ti*=1.5 and for a HDRB with *Ti*=1.5.

4.3 Influence of the number of layers in the isolator

As the number of layers increases, the elastic stiffness of the LRBs decreases significantly but the reduction is more rapid for the HDRB elastic stiffness; in contrast, the post-yield stiffness

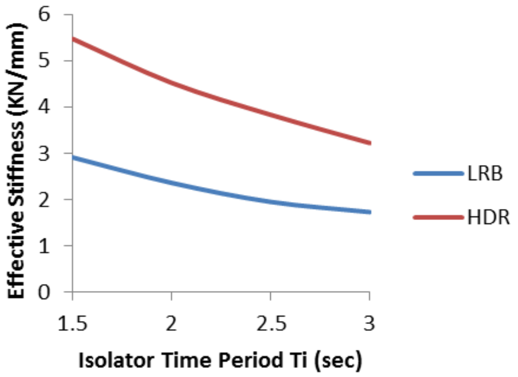

Fig. 13 Effective stiffness with isolator time period for LRB and HDRB

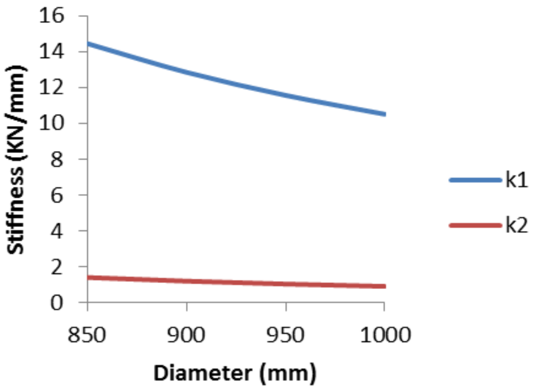

Fig. 14 Elastic stiffness and post-yielded stiffness with bearing size for LRB (Ti=1.5)

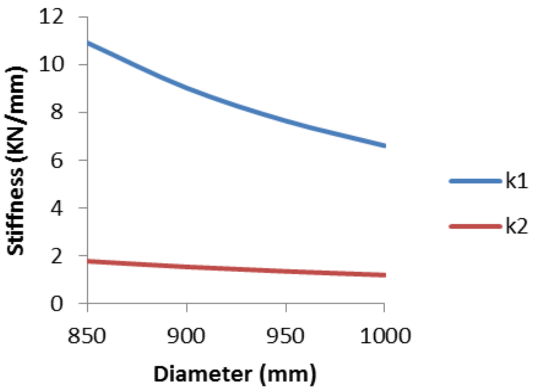

Fig. 15 Elastic stiffness and post-yielded stiffness with bearing size for HDRB (Ti=1.5)

decreases very slowly though in slightly higher amount for HDRB case. Fig. 18 and Fig. 19 illustrate how the stiffness varies with the number of layers for LRB (Qd=0.05) and HDRB respectively of Di=850 mm and Ti=1.5.

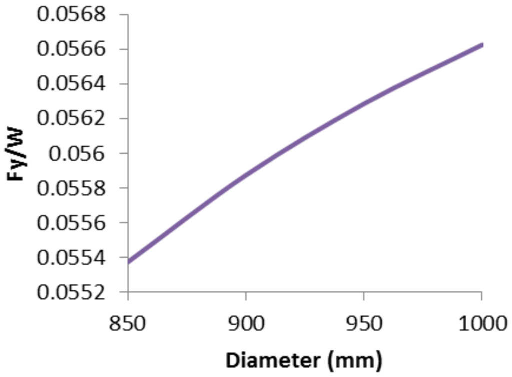

(a) for LRB (*Ti*=1.5)

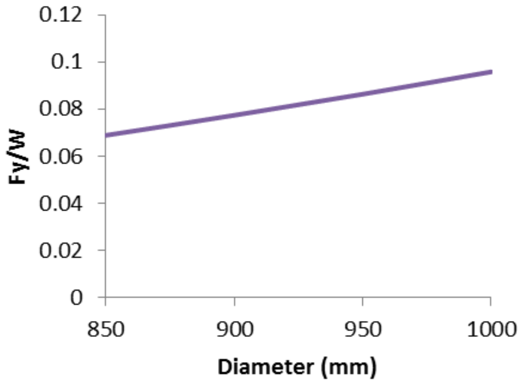

(b) for HDRB (*Ti*=1.5)

Fig. 16 Normalized yield force with bearing size

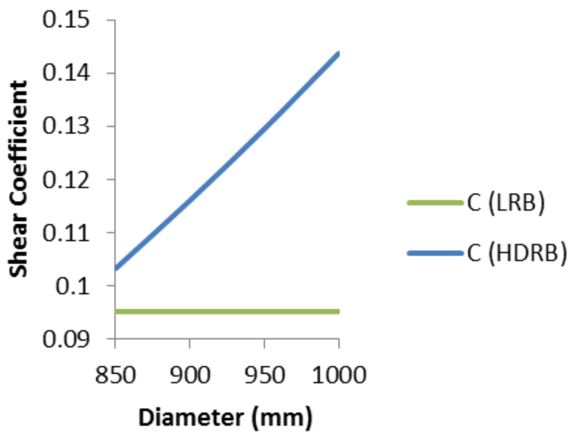

Fig. 17 Shear force coefficient/ normalized yield force with bearing size for LRB and HDRB

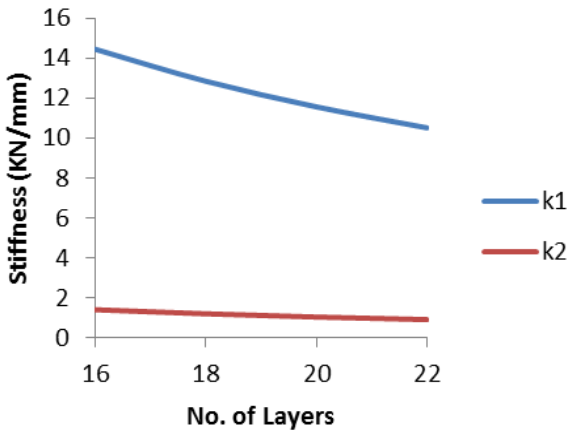

Fig. 18 Elastic stiffness and post-yielded stiffness with no. of layers of LRB (*Ti*=1.5, *Di* =850 mm)

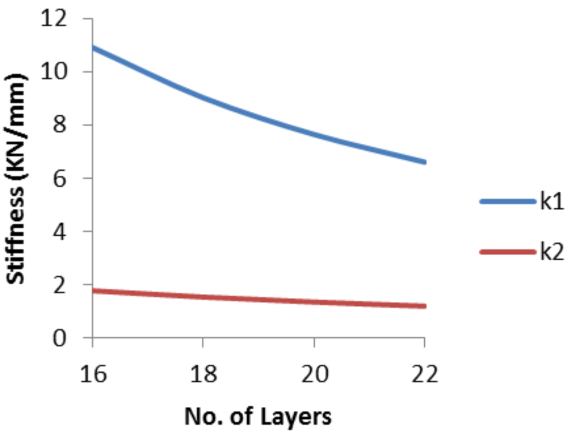

Fig. 19 Elastic stiffness and post-yielded stiffness with no. of layers of HDRB (*Ti*=1.5, *Di*=850 mm)

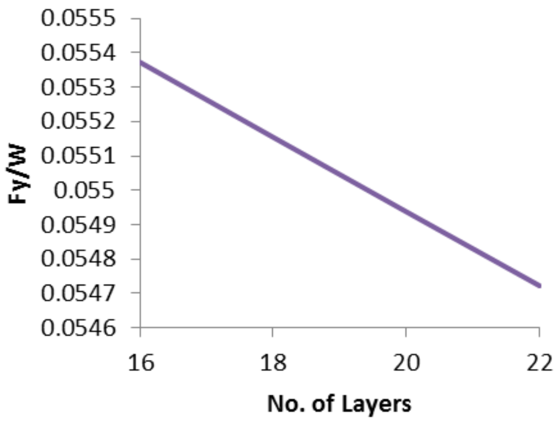

(a) LRB

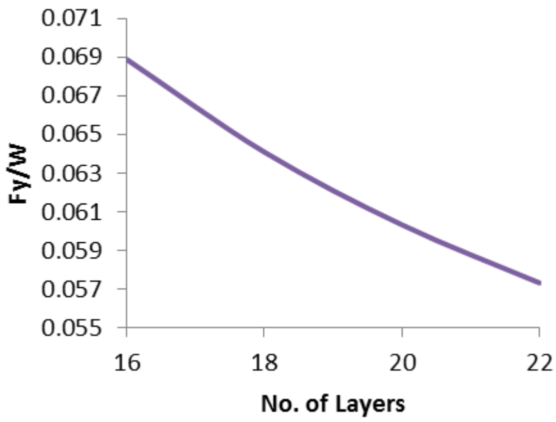

(b) HDRB

Fig. 20 Normalized yield force with no. of layers of bearing (*Ti*=1.5, *Di*=850 mm)

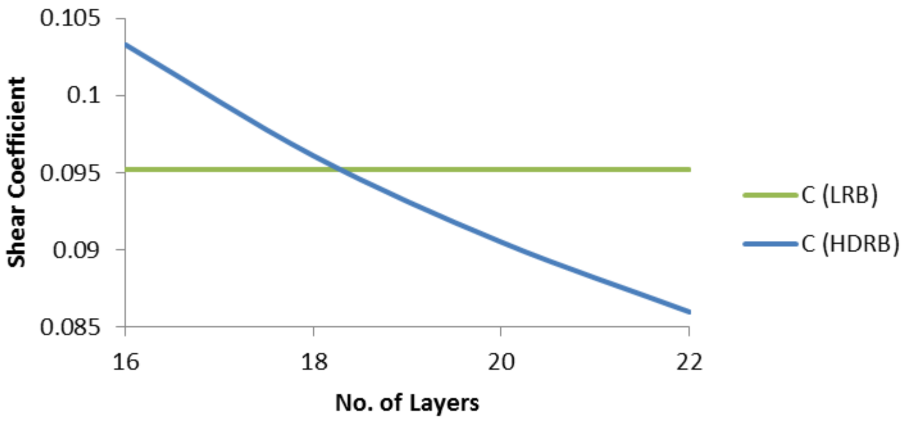

Fig. 21 Shear force co-efficient with no. of layers of LRB and HDRB

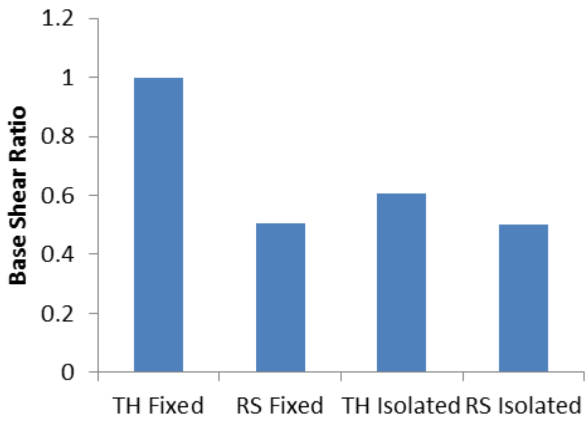

Fig. 22 Maximum base shear normalized to the maximum (fixed based) value

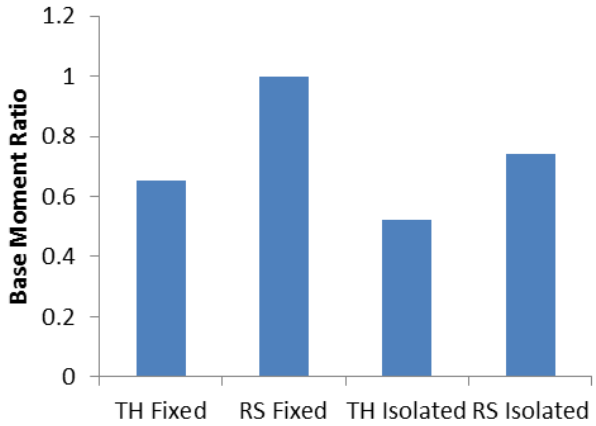

Fig. 23 Maximum base moment normalized to the maximum (fixed based) value

The normalized yield force decreases more linearly for an increasing number of layers for the LRBs than for the HDRBs. Fig. 20 illustrates how the normalized yield force varies with the number of layers in the isolated for a) a LRB with *Qd*=0.05 and *Ti*=1.5 and b) a HDRB with *Ti*=1.5.

Again, the base shear coefficients remain the same for all values of the diameter for the LRBs, whereas *C* decreases as the number of layers increases in the HDRBs. Fig. 21 presents the shear coefficients for a LRB with *Qd*=0.05 and *Ti*=1.5 and a HDRB with *Ti*=1.5.

4.4 Assessment of the response spectrum effect with the effect of time history

The performance of the RSB incorporation has been evaluated in terms of base shear (*V*) and base moment (M) which have been normalized with maximum shear and maximum moment respectively. Such the ratio of the V/V_{max} and M/M_{max} give a clear conception of lessening horizontal forces for structure retrofitting by RSB technique. When isolation is used, the base shear is reduced by 40% compared to the conventional structure. The maximum base moment is reduced by up to 24% for the isolated structure. Figs. 22 and 23 indicate that the base shear and base moment can be reduced for both the time history and response spectrum in terms of individual maximum values.

5. Conclusions

For existing multi-storied buildings, RSB base isolators could reduce the base shear up to 40-50% compared to the FB building. Furthermore, the base moment could be reduced by 25-45%. By and large, the rubber steel bearing reduces the structural responses significantly compared to the conventional non-isolated structures. Isolation allows for greater horizontal displacement and thus greater structural flexibility. The efficiency of isolator increases with increasing diameter and decreases with increasing number of layers. The suggested RSB isolation technique is able to mitigate the structural hazards of high seismic activity. Therefore, RSB isolators may be incorporated at the bottom of a superstructure to separate it from the sub-structure. This strategy is economical and increases the safety of the building.

This study dealt with the effectiveness of RSB in retrofitting the existing multistoried building but the construction aspects is still need to cover. Further study can be done for defining the proper construction method to install the base isolator without interrupting the studied parameter. Other models of isolators can also be investigated to get an optimum isolating system.

Acknowledgements

The authors gratefully acknowledge the support given by University of Malaya (UM) for funding the work through High Impact Research Grant H-16001-00-D000036.

Rerences

Ahmad, S., Ghani, F. and Raghib Adil, M. (2009), “Seismic friction base isolation performance using demolished waste in masonry housing”, *Constr. Build. Mater.*, **23**(1), 146-152.

Anzani, A., Binda, L., Carpinteri, A., Invernizzi, S. and Lacidogna, G. (2010), “A multilevel approach for the damage assessment of Historic masonry towers”, *J. Cultur. Heritage*, **11**(4), 459-470.

Ariga, T., Kanno, Y. and Takewaki, I. (2006), “Resonant behaviour of base-isolated high-rise buildings under long-period ground motions”, *Struct. Des. Tall Spec. Build.*, **15**(3), 325-338.

Ates, S. (2012), “Investigation of effectiveness of double concave friction pendulum bearings”, *Comput. Concrete*, **9**(3), 195-213.

Ates, S. and Yurdakul, M. (2011), “Site-response effects on RC buildings isolated by triple concave friction pendulum bearings”, *Comput. Concrete*, **8**(6), 693-715.

Bangladesh National Building Code (1993), *BNBC, Bangladesh: Housing and Building Research Institute*, Bangladesh Standard and Testing Institute.

Baratta, A. and Corbi, I. (2004), “Optimal design of base-isolators in multi-storey buildings”, *Comput. Struct.*, **82**(23-26), 2199-2209.

Betti, M. and Vignoli, A. (2011), “Numerical assessment of the static and seismic behaviour of the basilica of Santa Maria all’Impruneta (Italy) ”, *Constr. Build. Mater.*, **25**(12), 4308-4324.

Borzi, B., Vona, M., Masi, A., Pinho, R. and Pola, D. (2013), “Seismic demand estimation of RC frame buildings based on simplified and nonlinear dynamic analyses”, *Earthq. Struct.*, **4**(2), 157-179.

Casciati, F. and Hamdaoui, K. (2008), "Modelling the uncertainty in the response of a base isolator", *Probab. Eng. Mech*., **23**(4), 427-437.
Dall'Asta, A. and Ragni, L. (2006), "Experimental tests and analytical model of high damping rubber dissipating devices", *Eng. Struct.*, **28**(13), 1874-1884.
Dall'Asta, A. and Ragni, L. (2008), "Nonlinear behavior of dynamic systems with high damping rubber devices", *Eng. Struct.*, **30**(12), 3610-3618.
Dicleli, M. and Buddaram, S. (2007), "Comprehensive evaluation of equivalent linear analysis method for seismic-isolated structures represented by sdof systems", *Eng. Struct.*, **29**(8), 1653-1663.
Gürsoy, Ş. (2014), "Investigation of nonlinear behaviour of reinforced concrete frames having different stiffening members", *Comput. Concrete*, **13**(5), 679-694.
Habibullah, A. (2007), *ETABS: Three Dimensional Analysis of Building Systems*, Computers and Structures Inc. Berkeley, California.
Hong, W. and Kim, H. (2004), "Performance of a multi-story structure with a resilient-friction base isolation system", *Comput. Struct*., **82**(27), 2271-2283.
Iriarte, E., Sánchez, M.Á., Foyo, A. and Tomillo, C. (2010), "Geological risk assessment for cultural heritage conservation in karstic caves", *J. Cultur. Heritage*, **11**(3), 250-258.
Islam, A.B.M.S., Ahmad, S.I., Jameel, M. and Zamin, M. J. (2012a), "Seismic Base Isolation for Buildings in Regions of Low to Moderate Seismicity: Practical Alternative Design", *Prac. Period. Struct. Des. Constr.*, **17**(1), 13-20.
Islam, A.B.M.S., Hussain, R.R., Jumaat, M.Z. and Darain, K.M.U. (2014), "Implication of rubber- steel bearing nonlinear models on soft storey structures", *Comput. Concrete*, **13**(5), 603-669.
Islam, A.B.M.S., Hussain, R.R., Jumaat, M.Z. and Rahman, M.A. (2013a), "Nonlinear dynamically automated excursions for rubber-steel bearing isolation in multi-storey construction", *Auto. Construct.*, **30**, 265-275.
Islam, A.B.M.S., Jameel, M., Ahmad, S.I., Salman, F.A. and Jumaat, M.Z. (2011), "Engendering earthquake response spectra for Dhaka region usable in dynamic analysis of structures", *Scie. Res. Essay.*, **6**(16), 3519-3530.
Islam, A.B.M.S., Jameel, M., Jumaat, M.Z. and Rahman, M.M. (2013b), "Optimization in structural altitude for seismic base isolation at medium risk earthquake disaster region", *Disast. Adv*., **6**(1), 23-34.
Islam, A.B.M.S., Jameel, M., Uddin, M.A. and Jumaat, M.Z. (2012b), "Competent building elevation for incorporating base isolation in aseismic structure", *Procedia Eng.*, **50**(0), 882-892.
Islam, A.B.M.S., Jumaat, M.Z., Hussain, R. and Alam, M.A. (2013c), "Incorporation of rubber-steel bearing isolation in multi-storey building", *J. Civil Eng. Manag.*, **19**(sup1), S33-S49.
Ismail, M., Rodellar, J. and Ikhouane, F. (2010), "An innovative isolation device for aseismic design", *Eng. Struct.*, **32**(4), 1168-1183.
Khan, A.A. and Hossain, M.S. (2005), "Recurrence of 1885 Bengal earthquake and hazard vulnerability status of Dhaka Metropolitan City, Bangladesh", *Orient. Geograp.*, **49**(2), 205-216.
Kilar, V. and Koren, D. (2009), "Seismic behaviour of asymmetric base isolated structures with various distributions of isolators", *Eng. Struct.*, **31**(4), 910-921.
Lee, S.J., Lee, D.H., Kim, K.S., Oh, J.Y., Park, M.K. and Yang, I.S. (2013), "Seismic performances of RC columns reinforced with screw ribbed reinforcements connected by mechanical splice", *Comput. Concrete*, **12**(2), 131-149
Lu, L.Y. and Lin, G.L. (2008), "Predictive control of smart isolation system for precision equipment subjected to near-fault earthquakes", *Eng. Struct.*, **30**(11), 3045-3064.
Olsen, A., Aagaard, B. and Heaton, T. (2008), "Long-period building response to earthquakes in the San Francisco Bay Area", *Bul. Seismol. Soc. Am.*, **98**(2), 1047.
Ozmen, H.B., Inel, M. and Cayci, B.T. (2013), "Engineering implications of the RC building damages after 2011 Van Earthquakes", *Earthq. Struct*., **5**(3), 297-319.
Pocanschi, A. and Phocas, M.C. (2007), "Earthquake isolator with progressive nonlinear deformability", *Eng. Struct.*, **29**(10), 2586-2592.
Providakis, C.P. (2008), "Effect of LRB isolators and supplemental viscous dampers on seismic isolated

buildings under near-fault excitations", *Eng. Struct.*, **30**(5), 1187-1198.
Roy, B.K. and Chakraborty, S. (2013), "Optimal design of Base isolation System considering uncertain bounded system parameters", *Struct. Eng. Mech.*, **46**(1), 19-37.
Xue, X. and Yang, X. (2014), "Earthquake safety assessment of an arch dam using an anisotropic damage model for mass concrete", *Comput. Concrete*, **13**(5), 633-648.

CC

Appendix

Fig. A1 Front elevation view of the building

Fig. A2 Exterior corner fixed based column

Fig. A3 Fixed based column showing monolithic casting

Fig. A4 Interior fixed based column